Theor Chem Acc (2001) 105:345–353
DOI 10.1007/s002140000225

Theoretical
Chemistry Accounts

Regular article

Identification of molecular reactive sites with an interactive volume rendering tool

Preston J. MacDougall[1], **Christopher E. Henze**[2]

[1] Department of Chemistry, Middle Tennessee State University, Murfreesboro, TN 37132, USA e-mail: pmacdougall@mtsu.edu
[2] NASA Ames Research Center, MS T27A, Moffett Field, CA 94035, USA

Received: 1 June 2000 / Accepted: 4 October 2000 / Published online: 28 February 2001

Abstract. A new molecular visualization tool is presented, EVolVis (an abbreviation of electronic volume visualizer). This software enables the user to interactively explore a molecule's electronic charge density for topological features. Using novel volume rendering techniques, the entire molecule can be probed without obstruction by opaque surfaces or preselection of specific orbitals or contours. Menus with sliding scales permit various ranges of the function of interest to be examined interactively. We have investigated the Laplacian of the electronic charge density calculated for several biomolecules that contain a variety of reactive sites: cisplatin, penamecillin and isomers of nitrogen bases from DNA. EVolVis is useful in identifying inner-shell features (cisplatin), polar, nonpolar and aromatic regions (penamecillin), hydrogen-bonding sites of varying strength (nitrogen bases and penamecillin) and other reactive sites (strained heterocycle in penamecillin).

Key words: Laplacian – Hydrogen bonding – Volume rendering

1 Introduction

The electron density is ubiquitous in textbook expositions of various chemical phenomena. It is implicit in concepts ranging from "arrow-pushing" in physical organic chemistry to "Peierls distortions" in solid-state physics. In apparent contrast to its active rôles, the total electron density, ρ, is strongly dominated by mostly unchanging peaks that simply follow the nuclei during vibrations, as well as during chemical reactions. Except for bonds to hydrogen, the electron density near a bond "saddle" point is a fraction of 1% of its value at the nuclear positions. There are two basic approaches to addressing this "problem." The first approach is to select the "interesting" parts of the total electron density and to investigate them. The problem then becomes defining what is interesting, and with reference to the literature there are many responses found to be in practice. The second approach is to apply differential operators to the total electron density and to attempt to correlate the "uncovered" features with observed chemical behavior. The latter approach has been systematically applied to an ever-growing range of chemical phenomena since the pioneering work of Bader [1] over a quarter of a century ago. From these empirical roots, an extension of quantum mechanics to proper open systems, or atoms in molecules, has been developed [2, 3]. Here we present a new, interactive tool to assist with "data mining" in the vein of electron density analysis.

The Laplacian of the total electron density, $\nabla^2\rho$, exhaustively partitions a molecule into regions of local charge concentration ($\nabla^2\rho < 0$) and regions of local charge depletion ($\nabla^2\rho > 0$). This function has a shell structure that corresponds to the principal quantum shells in the electronic structures of both free atoms and atoms in molecules [4, 5]. The number, size and relative location of maxima in $-\nabla^2\rho$ that are found in the outermost shells, or valence-shell charge concentrations (VSCCs) of atoms in molecules [6], are accordant with Lewis' localized electron-pair model of electronic structure [7]. They also match the attributes of the postulated electron-pair domains of Gillespie's valence-shell electron-pair repulsion model of molecular geometry [8]. The number, size and relative locations of the charge depletions, or "holes" in the VSCCs of atoms in molecules, are predictive of possible sites of attack by nucleophiles, and the propensity for such reactivity [9, 10]. Such predictions can alternatively be made on the basis of Fukui's frontier orbital theory [11]; however, this approach encounters the problem of choosing among orbital models, and then possibly having to select a "frontier" orbital from among a dense set of low-lying virtual orbitals. The molecular visualization tools that

Contribution to the Proceedings of the 2000 Symposium on Chemical Bonding: State of the Art in Conceptual Quantum Chemistry

Correspondence to: P. J. MacDougall

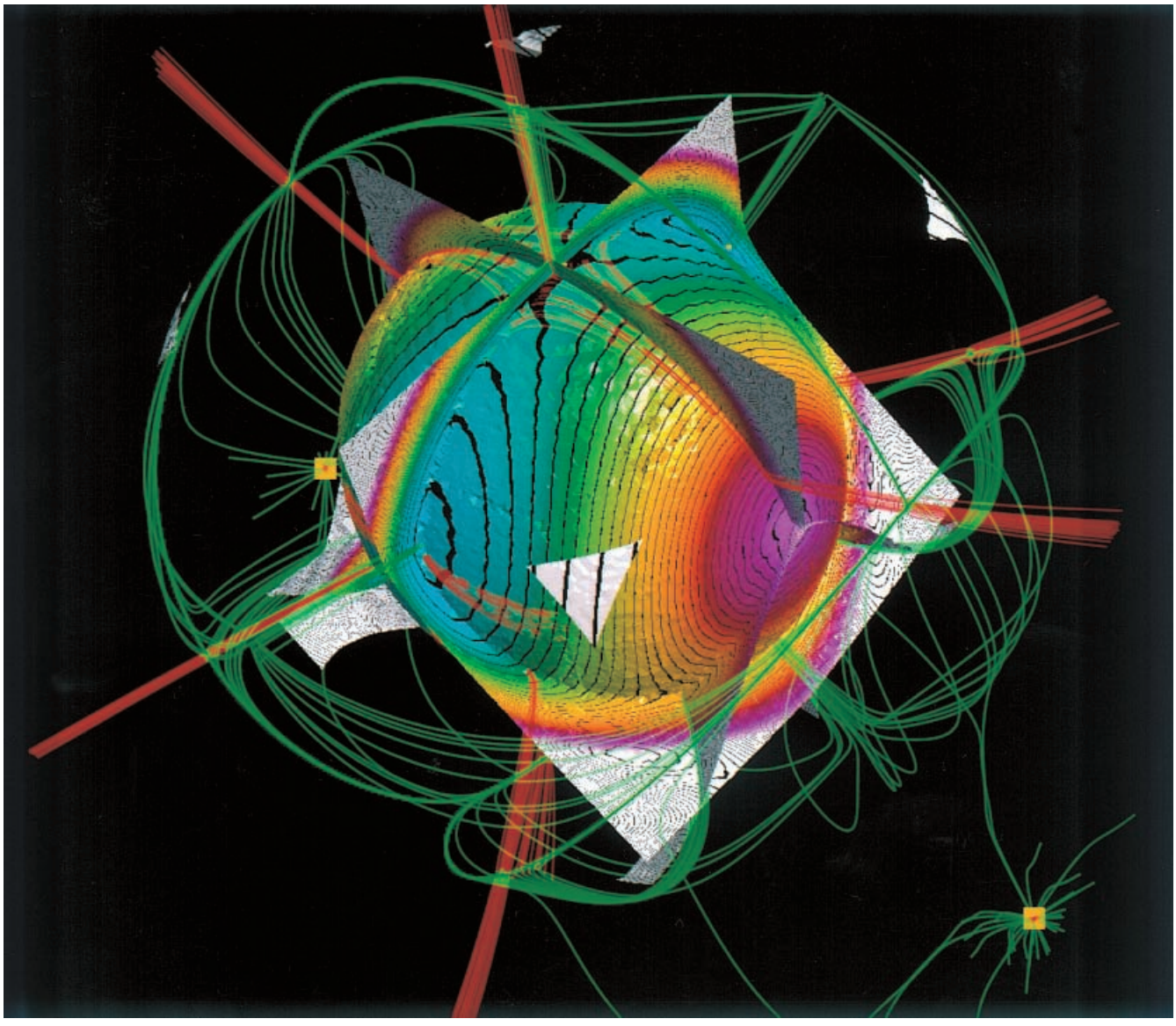

Fig. 1. Surface rendering of the extremal surface of the valence-shell charge concentration of oxygen in water and selected gradient trajectories (see text). The value of the Laplacian is negative everywhere on this surface; however, values become more negative as the color changes from *mauve* to *blue*

we discuss here share the common purpose of identifying and characterizing the reactive sites in molecules by topologically investigating $\nabla^2\rho$. The first method, employing "separation surfaces," specifically images the VSCC in a unique way, and also explicitly reveals the intricate connectivity of reactive sites (Fig. 1). The second method, employing "volume rendering," is an explorative tool, owing to its interactivity (Figs. 2–5). It is also capable of coarsely characterizing the chemical properties of an entire molecule, not just the reactive sites in the VSCC. These tools are discussed in further detail later, and their utility is demonstrated with applications to a variety of molecules.

An important outcome of this research into molecular visualization is the characterization of topological features in $\nabla^2\rho$ that are present at conventional hydrogen-bonding donor sites [12]. Owing to their similarity in appearance to skullcaps (Figs. 2, 4, 5), these features are named "yarmulkes".[1] The size of the yarmulkes at different sites increases with the expected strengths of the potential hydrogen bonds, given a similar acceptor such as water. In a study of hydrogen bonding between hydrogen fluoride and various bases, Carroll et al. [13] observed a critical point associated with this feature. The striking differences in the rendering of polar, nonpolar, aromatic and other chemically distinct regions of a molecule are also readily observed (Figs. 2, 4, 5). Identification of these diverse reactive sites is demonstrated and discussed in Sect. 3.

[1] Elsewhere we have used the Italian translation of skullcap, *papalina*

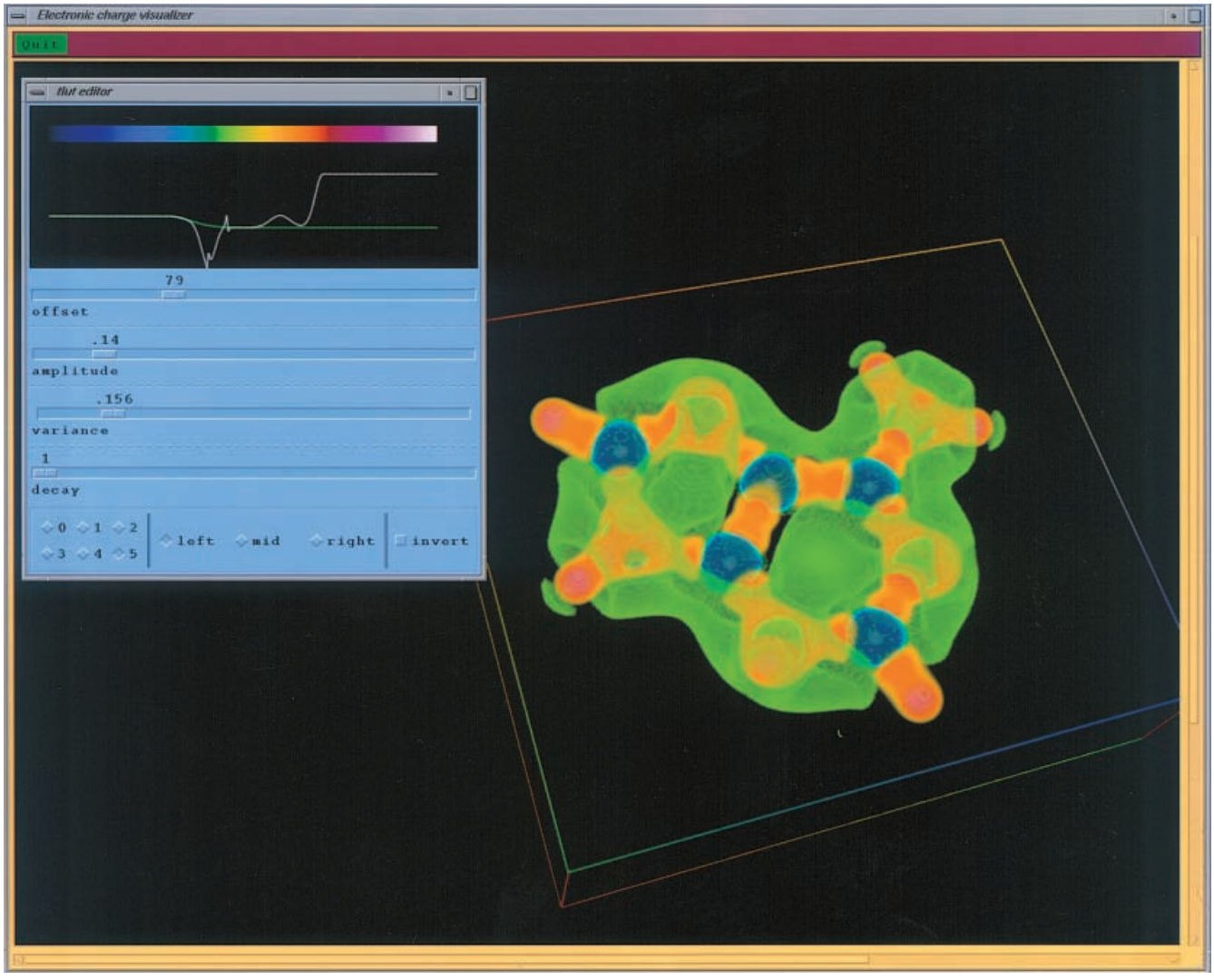

Fig. 2. A screenshot of the volume rendering of adenine, **2**, with EVolVis, including the window and menus for the transfer function editor. The *white line* in the editor window is the overall transfer function that was used to generate the rendering on the screen. The *green line* is the Gaussian that is currently being manipulated by the editor. It is shown clamped at the left (positive Laplacian). The *rainbow color scale* in the editor window (*violet* through *red*) corresponds to the Laplacian changing from positive to negative. The *green-to-yellow* transition corresponds to the Laplacian changing sign from positive to negative. *White* indicates extreme negative values of $\nabla^2\rho$, i.e. core concentrations of atoms. Aside from these traits, the color mapping is not constant for Figs. 2, 3, 4 and 5

The methods of displaying topological properties of ρ and $\nabla^2\rho$ that are presented here, and other related methods that are currently in use [2, 14–17], are, in principle, applicable to both theoretical densities (from quantum chemical calculations) and experimental densities (from X-ray diffraction) [18, 19]. The applications that we presently use for illustration are based on quantum chemical calculations.

2 Computational methods

2.1 Quantum chemical calculations

In all cases here, the electron densities are obtained from wavefunctions, in AIMPAC format [14], that have been computed with the GAUSSIAN ab initio quantum chemistry software package [20]. For cisplatin [*cis*-diamminedichloroplatinum(II)], **1**, the wavefunction was obtained from Pavankumar et al. [21]. This calculation was at the MP2/6-311G* level of theory, with an effective core potential on Pt (further details are available in Ref. [21]). All the nitrogen bases of DNA and RNA, adenine, **2**, thiamine, uracil, cytosine and guanine were examined with a new molecular visualization tool, EVolVis. We also examined selected isomers of guanine, in particular the *cis*-enol tautomer, **3**. All these calculations were done at the HF/6-311++G(2d,2p) level of theory, with geometry optimization at the same level. Finally, calculations were performed on penamecillin, **4**, an antibiotic [22], at the HF/6-311++G(1d,1p) level of theory. This calculation was done using the nuclear coordinates recently determined by Wagner et al. [23] in a high-resolution X-ray diffraction experiment at the DESY/HASYLAB synchrotron radiation source. The quantum chemistry calculations, on all but **1**, were done using desktop SGI workstations. The molecular visualizations were all done using SGI Onyx2 computers equipped with R10000 processors, InfiniteReality2 "KONAL" graphics boards and 64 MB of texture memory. EVolvis is written in C++, using OpenGL and the X Window system.

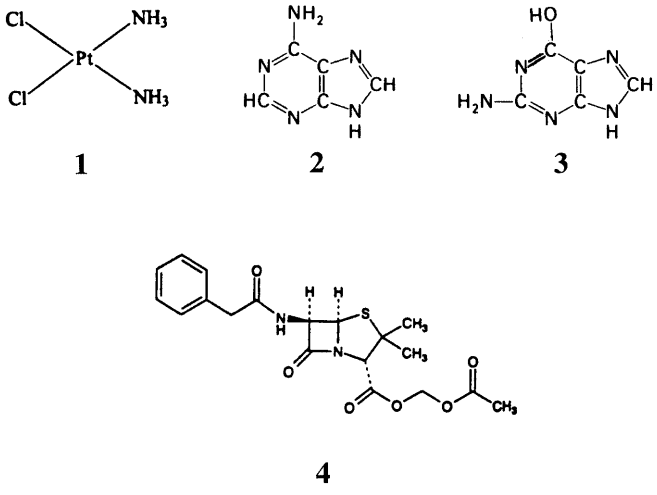

2.2 Separation surfaces

Natural and commonplace methods of graphical exploration of the scalar fields ρ and $\nabla^2\rho$ are with the aid of contour diagrams for a number of 2D planes, relief maps of such planar distributions and single-valued 2D surfaces or "envelopes." These afford an intuitive exploration of any scalar field. For further characterization, it is informative to explore the topology of these fields. We can do this by identifying features in the gradient fields of ρ and $\nabla^2\rho$; in particular, we wish to identify their critical points ($\nabla f = 0$) and certain zero-flux surfaces; namely, those zero-flux surfaces that contain the insets and outsets of the saddle points. These zero-flux surfaces constitute "basin boundaries" in the gradient fields. In the gradient field of ρ these basin boundaries constitute the interatomic surfaces of the quantum theory of atoms in molecules [2]. To explicitly image the extremal surface in the VSCC we need to locate critical points and separation surfaces in the gradient field of $\nabla^2\rho$.

Finding critical points and especially basin boundaries in a vector field is nontrivial. Related algorithms are employed to locate, and image, interatomic surfaces [14–17]. The approach we take here is straightforward, but computationally more intensive than locating interatomic surfaces. There are many more critical points in the Laplacian, and the gradients are frequently much larger, leaving less room for numerical imprecision. First, we

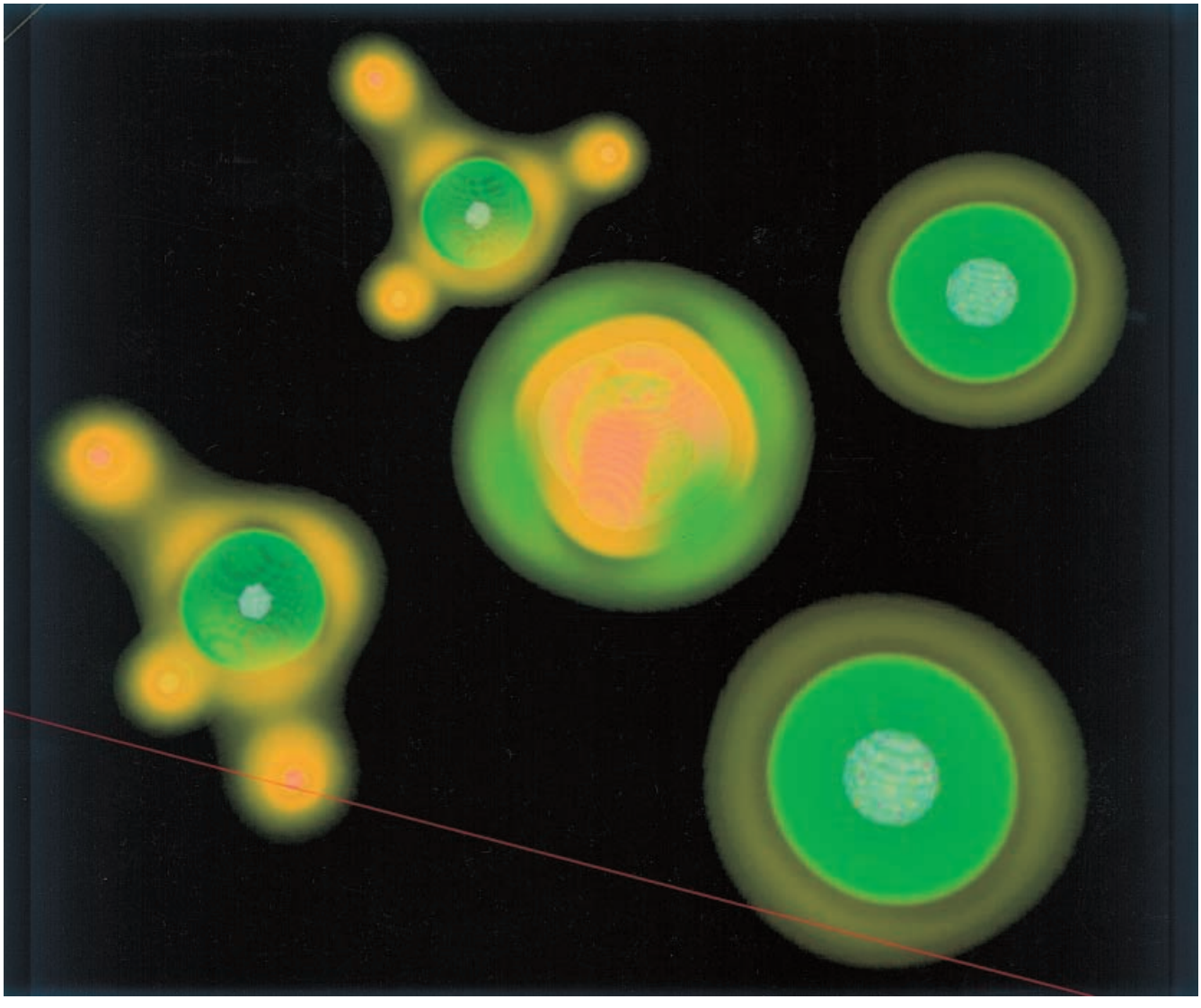

Fig. 3. Volume rendering of $\nabla^2\rho$ in cisplatin, **1**

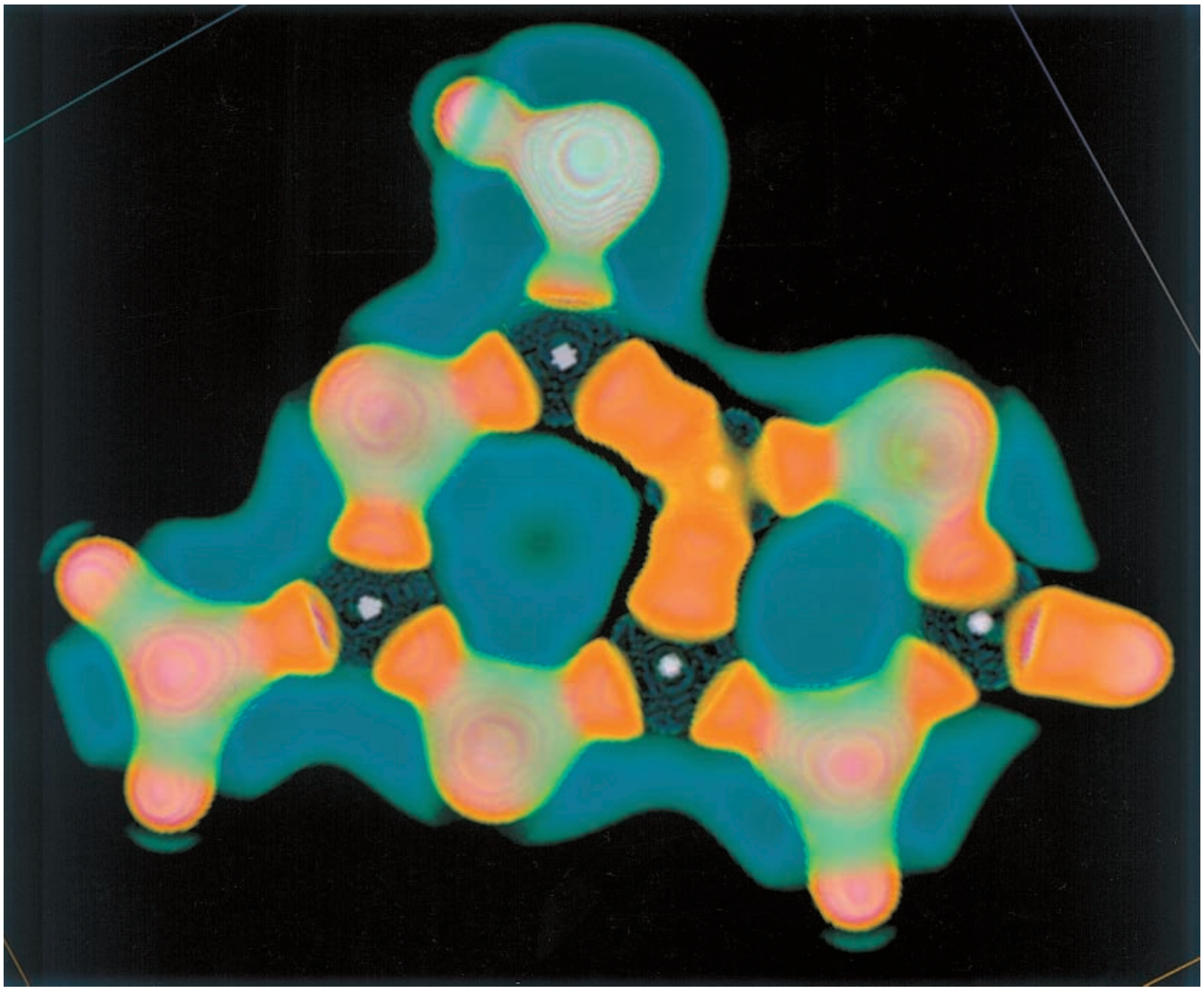

Fig. 4. Volume rendering of $\nabla^2\rho$ in 6-hydroxy-2-aminopurine, **3**

discretely sample the gradient field on a computational grid – this can be done either analytically from the wavefunction file or numerically by central differencing on the relevant discretized scalar field. Then, from each node of the grid, we follow integral curves in the gradient field until they either stagnate on a critical point or pass out of the domain. Integration is performed both forwards and backwards in the gradient field, so that repelling critical points and unstable saddle manifolds are identified, in addition to attracting critical points and stable saddle manifolds. In this way, we locate and classify all critical points, and we also determine which basin of attraction (or repulsion) each grid point "belongs to". Grid cells that contain adjacent vertices belonging to different critical points must be intersected by a separation (or attachment) surface, and this surface can be precisely located along grid cell edges by a simple bisecting search. All topological features in the VSCC lie on its extremal surface, wherein $\nabla^2\rho$ is a minimum with respect to displacement normal to this surface. This extremal surface is a separation surface in the gradient field of $\nabla^2\rho$. Alternatively, it can be said that the extremal surface in the VSCC is an attachment surface in the gradient field of $-\nabla^2\rho$. The values of the Laplacian at points on the separation surfaces are stored for later 2D surface rendering. Similarly, the direction of integration is stored for later color labeling of trajectories of $\nabla(\nabla^2\rho)$. Although this brute force method is computationally laborious, it can be optimized considerably by adopting a 3D analogue of graphical flood-fill algorithms. If a trajectory passes into a region of cells whose basin is already identified, the integration can be terminated. Therefore, regions of "known affiliation" can be grown outwards from critical points, and the total arc length of the integrations is greatly reduced.

The extremal surface in the VSCC of the oxygen atom in water appears in Fig. 1 as a brightly colored "marble" surrounded by a swarm of streamlines and sectioned by curved planes. The value of the Laplacian determines the color of the textured surface, which is also contoured to make the topology of the VSCC more evident. Since $\nabla^2\rho$ is negative everywhere on the VSCC, and has a relatively narrow range, a qualitatively different color scale is used here than in Figs. 2, 3, 4 and 5. The blue areas have the most locally concentrated charge (the nonbonded charge concentrations) and the red areas the least (the "faces" on the opposite side of the O–H bonds). The other planes are separation/attachment surfaces that are not part of the extremal surface in the VSCC. The streamlines are selected gradient vector trajectories. The green lines are those found by integrating forward, and they terminate at attractors in the gradient field of $\nabla^2\rho$. The red lines are found by integrating backwards, and they terminate at repellers in the gradient field of $\nabla^2\rho$ (some are seen terminating at a nonbonded concentration). The yellow squares that are attracting numerous green streamlines

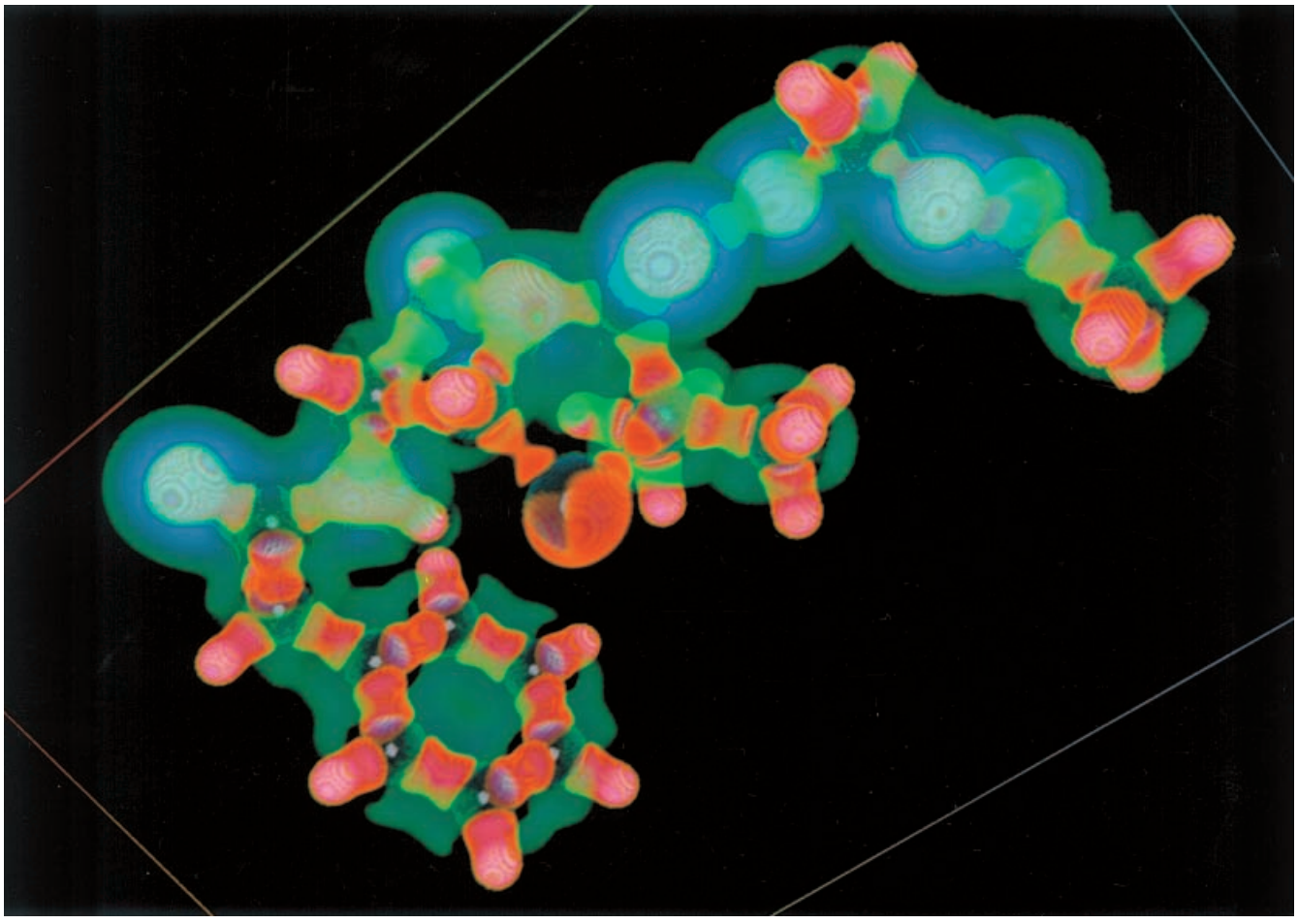

Fig. 5. Volume rendering of $\nabla^2\rho$ in penamecillin, **4**

are local charge depletions near the hydrogen nuclei (which are not imaged in this figure). These are the topological features that are associated with the hydrogen-bonding "yarmulkes" that are more fully characterized by the next visualization method that we present. Since hydrogen does not have a core, the "separation surface" associated with its "VSCC" is just a point at the maximum in ρ at, or very near, the hydrogen nucleus. This point is not imaged in Fig. 1 either.

2.3 Volume rendering

Even for a seemingly simple molecule such as water, the topology of the gradient field of $\nabla^2\rho$ is rich in structure, and there are numerous separation and attachment surfaces in addition to the extremal surface of the VSCC of oxygen (several are "clipped" in Fig. 1). This method of reactive site imaging is time consuming and requires substantial facility with topology on the part of the user. Neither is it efficient as a means of conveying information about a molecule's reactivity to a broad chemistry community (however, the images have been openly appreciated for their esthetic qualities). Similar imaging of a large biomolecule would be a challenge. Furthermore, it was necessary to clip portions of surfaces other than the VSCC because the outer surfaces would occlude the inner ones. These outer surfaces include the valence-shell charge depletion, which is where the critical points associated with the yarmulkes lie. This limitation is shared by all (2D) surface renderings of 3D objects. The $\nabla^2\rho = 0$ isovalued surface, or envelope, is often used to display the general form of the Laplacian distribution [2], and often the key topological features can be inferred from such an image. Frequently, however, the $\nabla^2\rho = 0$ envelope can be simple in appearance, masking important topological features inside. One may resort to a series of images of such envelopes, each with a different surface value. This is the 3D analogue of a contour diagram which has many contours. While a single contour diagram can easily be interpreted, it is much more difficult to collate a series of surfaces in one's mind. New "volume rendering" techniques in computer graphics offer a way to intuitively explore complex 3D distributions.

EVolVis uses volume rendering as its primary visualization technique. In our application, the volume rendering is implemented using 3D texture mapping, as originally suggested by Drebin in 1992 (cited by Haeberli and Segal [24]). The scalar data – electronic charge density or its Laplacian – are loaded into 3D texture memory, then slices through this volume perpendicular to the viewer are drawn and composited in back-to-front order. In addition to the viewpoint, the key user-controlled feature in this scheme is the transfer function, which maps the scalar volumetric data onto color and opacity values. By adjusting the transfer function, the user can highlight one or several value ranges in the data, in order to portray isosurfaces, interval volumes or smeared-out translucent "windows" in the data of interest.

The color transfer function is chosen from a set of predefined color maps. Typically, we use a standard "rainbow", which maps one extremum of the data onto blue (fading into black), then progresses through cyan, green, yellow, red, magenta and finally white, at the other extremum. The user can specify the extremal values, and any data outside these ranges are either clamped or ignored.

The real power of EVolVis derives from its opacity transfer function editor. This presents the user with a number of tunable Gaussian functions, $A\exp\{-[(x-B)/C]^D\}$, with slider controls for their amplitude (A), offset (B), variance (C) and decay rate (D).

Each Gaussian can also be clamped at its maximum value to the left or right of its peak, and each Gaussian can be inverted – an operation that simply flips the function over within its high and low range. Multiple Gaussians are superposed, allowing the user to create arbitrarily complex functions. The total resulting function maps data values onto opacities. Since the function editing and rendering is interactive, the user can rely on visual feedback to tune the transfer function and bring various data features into and out of focus. The input panel of the opacity function editor is shown in Fig. 2, with an example transfer function made up of several Gaussians.

The data that EVolVis uses to initialize 3D texture memory are generated from the AIMPAC format [14] wavefunction files produced by GAUSSIAN98. The approximation to the wavefunction is used to generate scalar values (usually electronic charge density, or its Laplacian – but any scalar value could be used) on a rectangular grid encompassing a region of interest within or around a molecule. The location, orientation and dimensions of the grid, and its regular lattice spacing in three directions, are specified by the user. We have found that good results are obtained with grid spacings of 0.05–0.10 Å. This means that a grid dimension of 256 represents 12.8–25.6 Å, which easily accommodates the longest axis of small molecules such as cisplatin, adenine, cytosine, thymine, guanine, uracil, penamecillin, etc. Of course, the grid dimensions can be made smaller in some directions, especially if the molecule is flat. A volumetric data set of 256^3 8-bit values requires 16 MB of texture memory, well within the 64 MB texture memory limit of our machines. Data sets larger than this require paging in and out of texture memory, which greatly reduces interactivity.

Figure 2 is a computer screenshot of adenine, **2**, being rendered with EVolVis. Compared to the generation of informative trajectories and separation surfaces in the gradient field of $\nabla^2\rho$ (Fig. 1), data mining for reactive sites with volume rendering is intuitive and easy to master. We venture to say that it is even fun to interactively explore the "lumps and holes" in molecular charge distributions that are a result of sculpting by electrostatic and quantum forces. One can readily observe the green yarmulkes behind the hydrogens (the red "thumbs") at the three hydrogen-bonding donor sites, one at N9 (bottom left) and two at the amino group (top right). The C–H bonds are noticeably capless. In this one image, the qualitative features of the VSCCs of the atoms are also evident. The red nonbonding charge concentrations of the more basic imino nitrogens (N1, N3 and N7) are prominently directed outward. The susceptibility to nucleophilic attack of the five carbons is apparent from their more exposed core depletions (blue balls). The white core charge concentrations are still visible for all the carbon atoms and some of the nitrogens, even though the valence features were the objects of focus. In cases where one wishes to determine relative reactivities of the similar atoms, such as which carbon is most susceptible to nucleophilic attack, then the transfer function can easily be tuned for that purpose. By saving scripts of the transfer function optimization, EVolVis can be used to systematically examine a series of related molecules for trends in reactivity.

3 Applications and discussions

3.1 Transition-metal complexes; cisplatin

In transition-metal complexes, topological features in $\nabla^2\rho$ that are dependent on "*d*-electron count" are found in the same shell of charge concentration as would be considered the outer shell of the core [25]. For instance, manganese is a fourth-row element which, in $Mn_2(CO)_{10}$, has "valence" charge concentrations in both its third (inner valence) and fourth (outer valence) shells of charge concentration [26] (labeled i-VSCC and o-VSCC, respectively [27]). The o-VSCC is often lost in charge-transfer complexes, such as cisplatin, **1** (Fig. 3), and other transition-metal complexes where the outer valence electrons are said to be "promoted to *d* orbitals." The topology of the i-VSCC determined from X-ray charge density studies of $Mn_2(CO)_{10}$ [28] agrees with the ab initio results referred to earlier; however, the single charge concentration in the o-VSCC (at the midpoint of the Mn–Mn bond) was not observed. This is a reflection of the virtual "flatness" of the charge density at this site, $\nabla^2\rho = 1.21$ e/Å^5 (experiment) versus -0.14 e/Å^5 (theory), rather than a strong disagreement between experiment and theory. For comparison, the charge concentrations in the i-VSCC of manganese have $\nabla^2\rho$ values in the range -600 to -800 e/Å^5, which is indicative of their partial "corelike" character. The charge concentrations in the VSCCs of the ligands may have $\nabla^2\rho$ values ranging from -25 e/Å^5 (carbon) to -150 e/Å^5 (oxygen). As discussed previously, the orders-of-magnitude differences in such topological features would require numerous 2D surface renderings, whereas volume rendering can image them all at once. Furthermore, there are 32 orbitals that significantly contribute to the VSCCs in cisplatin, which is exceptionally simple among bioinorganic complexes. Again, the "wholeness" of volume rendering offers a tremendous advantage over piecemeal methods. We illustrate these distinctions with cisplatin in Fig. 3.

The ab initio calculations by Pavankumar et al. [21] employed effective core potentials. This is why a small white ball is not seen at the core of the central platinum atom, while balls are seen for nitrogen and chlorine (the ball is bigger since the core of chlorine has ten electrons versus nitrogen's two). The much greater extent of the "corelike" nonbonded charge concentrations in the i-VSCC of platinum (four red lobes) is in clear contrast to the more diffuse features in the VSCC of nitrogen and chlorine. One can see that the maximum extent of charge concentration in platinum's i-VSCC is similar to that found in the vicinity of the hydrogen nuclei. Also, the extent of charge depletion in the green clover leaf encircling platinum's i-VSCC (corresponding to the vacant $d_{x^2-y^2}$ orbital in the ligand-field model of its electronic structure) is comparable to the charge depletions seen only in the core depletions of nitrogen and chlorine. This extent of charge depletion is not reached in the valence depletions of nitrogen or chlorine. These electrophilic reactive sites, or "holes" in the coordination sphere of platinum (which is a shell of charge depletion), are clearly aligned with the yellow coordinating charge concentrations on the ligands. The angle formed by these topological features opposite the chlorine ligands is predictive of the preferred "bite angle" of the chelation complex formed when cisplatin binds to the N7s of adjacent intrastrand guanine or adenine bases in DNA [29]. The corresponding "lump" in the image of adenine in Fig. 2 is the nonbonding charge concentration of the imine nitrogen in the five-membered ring (top left).

3.2 Nitrogen bases: adenine, guanine, etc. and selected isomers

Using EVolVis, we scanned the computed $\nabla^2\rho$ distributions for reactive sites in adenine (Fig. 2), thymine,

uracil, cytosine and guanine. In all cases yarmulkes were found at the expected hydrogen-bond donor sites, but not at any other hydrogen atoms. In addition to the lack of topological features associated with hydrogen bonding (and the number of hydrogens), there is a contrast in the overall rendering of the methyl group in thymine, as compared to the amine groups of adenine, guanine and cytosine (and also the ammonium groups of their protonated forms). This ready discrimination between chemically distinct functional groups (without any labels) is a nontrivial capability of this method of volume rendering, and we discuss it further in the next section. Here we focus on the identification, and properties, of reactive sites associated with hydrogen bonding.

The *cis*-enol tautomer of guanine, **3**, has four types of hydrogens: amino (primary and secondary), hydroxy and vinyl. All but vinyl are conventional hydrogen-bond donors, and a ''yarmulke'' identifies the charge depletions that impart their selective reactivity (Fig. 4). The amino sites are similar, but the hydroxy site is greater in size and extent of charge depletion. These physical characteristics are consistent with trends in hydrogen-bonding strengths [12]. The lack of a yarmulke near the vinyl hydrogen is not simply a result of the specific transfer function used in the volume rendering. At the corresponding site in vinyl hydrogens there is a local *minimum* in charge depletion, while a yarmulke contains a local *maximum* in charge depletion. Further investigations of C–H bonds with EVolVis have shown that the substituents bonded to carbon can alter the topology of the region of charge depletion behind the hydrogen. In particular, all three hydrogens in methyl fluoride have yarmulkes, although they are not as pronounced as those in Fig. 4.

A growing number of types of noncovalent interactions are being utilized in supramolecular engineering [30], and C–H fragments in particular are considered as potential, albeit weak, hydrogen-bond donors [31]. The abundance of such potential sites in any organic material emphasizes the demand for means of identifying and characterizing such sites, when in fact they exist. EVolVis shows potential utility in this regard, although more systematic studies are needed on a wider variety of organic systems. Hobza et al. [32] have postulated ''improper, blue-shifted'' hydrogen bonding, defined as a lengthening of the C–H (donor) bond and a blue-shift of its stretching frequency. They have observed good correlations between these changes and the topological properties of the resulting bond critical points. EVolVis should prove useful in a priori identification of the potential sites of such novel interactions. Platts [33] has found correlations between integrated properties associated with the hydrogen-bond donor site and hydrogen-bond donor capacity. The local charge depletions identified by the yarmulkes provide a complementary means of characterizing these reactive sites that are key to both structure and function in biomolecules.

3.3 Medicinal compounds: penamecillin

The versatility of EVolVis is demonstrated in Fig. 5. With one easily optimized transfer function, key reactive sites are identified and the penamecillin molecule, **4**, is partitioned into chemically distinct fragments, simultanesously. The reactive ''pocket'' near the middle of the molecule shows the proximity of the orange–red nonbonded charge concentrations (associated with lone pairs) on sulfur and the lone yarmulke behind the hydrogen of the amide group (the only conventional hydrogen-bond donor in this molecule). The polar nature of the diester side chain (top right) is clearly differentiated from the nonpolar aryl group at the opposite end of the molecule. Even the methyl and methylene groups in the polar region are easily identified. The transfer function can readily be modified to focus on the numerous hydrogen-bond acceptor sites in this molecule. The orientation of penamecillin in Fig. 5 does not offer a good view of the lactam ring, but does show the thia-substituted ring side on, revealing an interesting asymmetry in the charge concentrations associated with the two carbon–sulfur bonds (one bonded charge concentration is clearly seen as contiguous, the other ''severed''), possibly resulting from uneven distribution of ring strain. This is in agreement with X-ray charge density studies by Wagner et al. [23]. Storing the rendering in texture memory allows rapid molecular rotations. So doing clearly reveals the bulbous nonbonding charge concentration on the bridgehead nitrogen (seen shrouded in Fig. 5) as well as the ''holes'' in the VSCC of the amide carbon.

4 Summary

The new methods of molecular visualization that we have presented conveniently differentiate molecular fragments and can identify both expected as well as unexpected reactive sites. This is not done with ''rule-based'' algorithms, but rather with direct examination of the observable charge distribution, à la Bader. Thus, we expect that it will prove useful in the chemical characterization, or design, of complex molecules that possess, or require, both conventional and unconventional reactive sites.

In conclusion, we have added new wrinkles to an old irony, one that was noted by Lewis in 1938 [34]. He observed ''It is always of interest to find that some of our most modern scientific ideas have been vaguely anticipated by scientists of earlier centuries. One of the ideas of Lemery, a contemporary of Robert Boyle, is amusingly discussed in a well known history of chemistry, as follows: 'Yet one of his theoretical conceptions was very odd, and shows how far astray a capable man may wonder, when he deserts observed facts for philosophical speculations. He thought that chemical combination between two substances, such as an acid and a base, might be accounted for by supposing that the particles of the one were sharp, and those of the other porous, and

that chemical combination was effected by the fitting of the points into the holes!'''

Acknowledgements. This research was conducted at the NASA Ames Research Center, where P.J.M. was supported by a NASA-ASEE-Stanford Summer Faculty Fellowship.

References

1. Bader RFW (1975) Acc Chem Res 8: 34
2. Bader RFW (1990) Atoms in molecules: a quantum theory. Clarendon, Oxford
3. Bader RFW (1994) Phys Rev B 49: 13348
4. Bader RFW, Essén H (1984) J Chem Phys 80: 1943
5. Sagar RP, Ku ACT, Smith VH, Simas AM (1988) J Chem Phys 88: 4367
6. Bader RFW, MacDougall PJ, Lau CDH (1984) J Am Chem Soc 106: 1594
7. Lewis GN (1916) J Am Chem Soc 38: 762
8. Gillespie RJ, Hargittai I (1991) The VSEPR model of molecular geometry. Allyn and Bacon, Boston
9. Bader RFW, MacDougall PJ (1985) J Am Chem Soc 107: 6788
10. MacDougall PJ, Bader RFW (1986) Can J Chem 64: 1496
11. Fukui K (1971) Acc Chem Res 4: 57
12. Jeffrey GA, Saenger W (1994) Hydrogen bonding in biological structures. Springer, Berlin Heidelberg New York
13. Carroll MT, Chang C, Bader RFW (1988) Mol Phys 63: 387
14. Bader RFW (1999) AIMPAC programs. www.chemistry.mcmaster.ca/aimpac/
15. (a) Popelier PLA (1996) Comput Phys Commun 93: 212; (b) Popelier P (2000) Atoms in molecules: an introduction. Pearson Education, Harlow, UK; (c) MORPHY98. www.ch.umist.ac.uk/morphy/
16. (a) Luaña V, Costales A, Martín Pendás A (1997) Phys Rev B 55: 4285; (b) Martín Pendás A, Luaña V (1995) CRITIC program, contact author at angel@carbono.quimica.uniovi.es; (c) Luaña V (1996) TESSEL 2.0. www.uniovi.es/quimica.fisica/qcg/programs/tessel.html
17. (a) Gatti C, Saunders VR, Roetti C (1994) J Chem Phys 101: 10686. Gatti C, Cargnoni F (1996) TOPOND program, contact author at c.gatti@csrsrc.mi.cnr.it
18. (a) Koritsanszky T, Flaig R, Zobel D, Krane H-G, Morgenroth W, Luger P (1998) Science 279: 356; (b) Koritsanszky T, Howard S, Mallinson PR, Su Z, Richter T, Hansen NK (1998) XD charge density package, contact author at tibor@hobbes.gh.wits.ac.za
19. (a) Craven BM, Stewart RF (1990) Trans Am Crystallogr Assoc 26: 41; (b) Stewart RF, Spackman MA (1981) VALRAY user's manual. Chemistry Department, Carnegie Mellon University, Pittsburgh, Pa
20. Frisch MJ, Trucks GW, Schlegel HB, Scuseria GE, Robb MA, Cheeseman JR, Zakrzewski VG, Montgomery JA, Stratmann RE, Burant JC, Dapprich S, Millam JM, Daniels AD, Kudin KN, Strain MC, Farkas O, Tomasi J, Barone V, Cossi M, Cammi R, Mennucci B, Pomelli C, Adamo C, Clifford S, Ochterski J, Petersson GA, Ayala PY, Cui Q, Morokuma K, Malick DK, Rabuck AD, Raghavachari K, Foresman JB, Cioslowski J, Ortiz JV, Stefanov BB, Liu G, Liashenko A, Piskorz P, Komaromi I, Gomperts R, Martin RL, Fox DJ, Keith T, Al-Laham MA, Peng CY, Nanayakkara A, Gonzalez C, Challacombe M, Gill PMW, Johnson BG, Chen W, Wong MW, Andres JL, Head-Gordon M, Replogle ES, Pople JA (1998) GAUSSIAN98. Gaussian, Pittsburgh, Pa
21. Pavankumar PNV, Seetharamulu P, Yao S, Saxe JD, Reddy DG, Hausheer FH (1999) J Comput Chem 20: 365
22. Russell J (1965) J Chem Soc: 2127
23. (a) Wagner A, Bombicz P, Flaig R, Luger P (1999) Acta Crystallogr A 55S: 514; (b) Wagner A (1999) Thesis. Institute for Crystallography, Free University of Berlin
24. Haeberli P, Segal M (1993) www.sgi.com/grafica/texmap/index.html
25. (a) MacDougall PJ, Hall MB (1990) Trans Am Crystallogr Assoc 26: 105; (b) Gillespie RJ, Bytheway I, Tang TH, Bader RFW (1996) Inorg Chem 35: 3954
26. MacDougall PJ (1989) PhD dissertation. Department of Chemistry, McMaster University, Hamilton
27. MacDougall PJ, Hall MB, Bader RFW, Cheeseman JR (1989) Can J Chem 67: 1842
28. Bianchi R, Gervasio G, Marabello D (1998) Chem Commun 1535
29. Fichtinger-Schepman AMJ, Lohman PHM, Reedijk J (1982) 10: 5345
30. Desiraju GR, Steiner T (1999) The weak hydrogen bond in structural chemistry and biology. Oxford University Press, New York
31. Desiraju GR (1991) Acc Chem Res 24: 290
32. Hobza P, Spirko V, Selzle H, Schlag E (1998) J Phys Chem A 102: 2501
33. Platts JA (2000) Phys Chem Chem Phys 2: 973
34. Lewis GN (1938) J Franklin Inst 226: 293